



Research Article

## Effects of gas-liquid flow and dehumidification performance of a liquid desiccant dehumidifier: A numerical approach for vertical smooth & rough, and inclined rough plates

Md. Tamzid SHAHARIER<sup>1</sup>, Dipayan MONDAL<sup>1,\*</sup>, Md. Abdul HASIB<sup>1</sup>, Md. Ashraful ISLAM<sup>1</sup>

<sup>1</sup>Department of Mechanical Engineering, Khulna University of Engineering & Technology, Khulna, 9203, Bangladesh

### ARTICLE INFO

#### Article history

Received: 06 April 2024

Revised: 04 August 2024

Accepted: 04 August 2024

#### Keywords:

Dehumidifier Performance;  
Heat and Mass Transfer; Liquid  
Desiccant; Moist Air; Vertical  
and Inclined Plates

### ABSTRACT

This study investigates the dehumidification performance and the gas-liquid flow of a falling film liquid desiccant dehumidifier with different plate configurations: vertical smooth, vertical rough, and inclined rough. Utilizing ANSYS Workbench 2020 R1, the Re-Normalization Group (RNG) k- $\epsilon$  turbulence model has been utilized to simulate the gas-liquid flow, and the volume of fluid model is employed to track the interface patterns between the gas and liquid phases. This model takes into account the effects of the two-dimensional turbulent flow which is performed for various plate configurations under situations of unstable gas-liquid flow. The 30% LiCl solution is used as an absorbent and hence, the performance has been evaluated using a constant mass transfer rate of 50 mol/s. Furthermore, the LiCl solution's mass concentration is taken into account as 30%, 33%, 36%, 40%, and 44%, respectively, for the justification of the influence of various concentrations of LiCl solution. The study analyzes the fields of mass fractions and the mechanisms that lead to the enhancement of dehumidification. The research examines the influence of inlet desiccant concentration and air velocity on mass transfer properties, revealing that an inclined ribbed plate significantly enhances dehumidification up to 10.8% compared to the smooth plate particularly at 1.5 m/s inlet air velocity by generating liquid film waves and increasing contact time between the liquid desiccant and moist of air. Lower inlet air velocities and higher inlet desiccant concentrations resulted in a decreased outlet mass percentage of water vapor. The optimal LiCl concentrations for water vapor absorption are 30-40%, with efficiency stable above 36%, though benefits may plateau beyond a certain level. The study concludes that the inclined rough plate enhances mass transfer performance at various inlet air velocities and desiccant concentrations by increasing the contact time between the liquid desiccant and moist air, increasing the rate of water vapor absorption. These findings provide valuable insights for researchers and engineers aiming to optimize liquid desiccant dehumidification systems for various applications, especially in the hybrid liquid desiccant-vapor compression systems.

**Cite this article as:** Shaharier MT, Mondal D, Hasib MA, Islam MA. Effects of gas-liquid flow and dehumidification performance of a liquid desiccant dehumidifier: A numerical approach for vertical smooth & rough, and inclined rough plates. J Ther Eng 2024;10(6):1559–1576.

#### \*Corresponding author.

\*E-mail address: [dipkuet@me.kuet.ac.bd](mailto:dipkuet@me.kuet.ac.bd)

*This paper was recommended for publication in revised form  
by Editor-in-Chief Ahmet Selim Dalkılıç*



## INTRODUCTION

Nowadays, liquid desiccant air conditioning (LDAC) systems and other dehumidification systems use a liquid desiccant to remove moisture and heat from the air to improve the air quality, which can result in significant energy savings. The liquid desiccant dehumidifier (LDD) is a vital part of LDAC systems that act as a heat and mass exchanger that removes moisture from the air as it passes over plates coated with liquid desiccant. The liquid desiccant regenerator (LDR) then removes the absorbed moisture from the desiccant, allowing it to be reused. Common liquid desiccants used in LDAC systems include lithium bromide (LiBr), calcium chloride (CaCl), and lithium chloride (LiCl). On the contrary, solid desiccant cooling systems use materials like silica gel or zeolites to absorb moisture from the air at lower temperatures, requiring separate heating for regeneration. They offer lower corrosion risk and potential energy efficiency benefits but can be costly initially. Therefore, liquid desiccant cooling systems use solutions such as lithium chloride for faster moisture absorption, requiring higher regeneration temperatures and careful material selection to avoid corrosion. They provide flexibility in heat sources but may have higher operational energy costs. In general, liquid desiccants play an important role in improving indoor air quality, reducing energy consumption, and improving the efficiency of air conditioning and dehumidification systems [1]. However, lithium chloride (LiCl) is a highly hygroscopic substance that readily absorbs water vapor from the air. The mechanism by which a LiCl solution absorbs water vapor through the process of water vapor diffusion, where the water vapor molecules in the air move from areas of higher concentration to areas of lower concentration. The computational fluid dynamics (CFD) analysis of a liquid desiccant dehumidifier was performed by Lu and Lu [2] and enhancing the dehumidification performance of LiCl solution was investigated by Wen et al. [3]. When a LiCl solution is exposed to air, the water vapor molecules in the air diffuse into the solution, attracted by the high concentration of water molecules in the LiCl solution. As the water vapor molecules diffuse into the LiCl solution, they bond with the lithium cations (Li<sup>+</sup>) and chloride anions (Cl<sup>-</sup>) in the solution to form a stable hydrated complex. This process continues until the concentration of water vapor in the air and the solution reaches equilibrium, at which point the solution is said to be saturated with water vapor [4]. The extent to which a LiCl solution absorbs water vapor depends on several factors, including the concentration of the solution, the surface area of the exposed solution, and the relative humidity of the surrounding environment. The more concentrated the solution, the more water vapor it can absorb. Similarly, the greater the surface area of the exposed solution, the more water vapor it can absorb. In a high-humidity environment, the LiCl solution will

absorb more water vapor than in a low-humidity environment [5]. In the meanwhile, Zhang et al. [6] studied the shrinkage of a liquid film running downhill down the heated solid surface, which results from the presence of a surface tension gradient and is significantly impacted by the Marangoni effect. Another study by Zhang et al. [7] optimized the operating parameters of a LiCl dehumidification system, including the concentration of the LiCl solution and the regeneration temperature, to maximize its performance. They found that a concentration of 60 % and a regeneration temperature of 70 °C resulted in the best performance. Das and Jain [8] investigated solar energy utilization as a heat source for the regeneration of a LiCl dehumidification system. They found that the use of solar energy reduced the energy consumption of the system and increased its overall efficiency. While Zhang et al. [9] conducted the exergy calculation and analysis of a dehumidification system using LiBr liquid desiccant.

A study by Chen et al. [10] analyzed temperature and humidity with incorporated dehumidification technology. Air dehumidification employs low-temperature, low-concentration liquid desiccant; condensation heat may be used to resupply the desiccant solution. Stevens et al. [11] outlined a computationally effective model for mass and heat exchangers with packed beds and liquid desiccant that encompasses the creation and extraction of the efficacy model, testing against experimental data, and a finite-difference model. A study by Liu et al. [12] proposed a new model that incorporated a heat pipe for heat recovery and a multistage configuration for improved dehumidification performance. The liquid film in the LDD is very thin, making it challenging to measure the properties of the film and accurately predict dehumidification operations [13]. Earlier studies have used the NTU model [14] and the finite difference model [15] to obtain results. Nevertheless, a CFD analysis [12] was performed on smooth plates to express the dehumidification process of LDDs, and it successfully predicted the heat and mass transfer characteristics. Liu et al. [16] presented the results of a study on the mass transfer capabilities of a cross-flow dehumidifier employing a liquid desiccant. The dehumidifier was equipped with Celdek structured packings, and the liquid desiccant was an aqueous solution of LiBr. Tao et al. [17] reported an investigation of the liquid desiccant dehumidification process based on CFD technology and Wen et al. [3] also reported the enhancement of the ability of the LiCl solution dehumidification process with surfactant Polyvinylpyrrolidone (PVP) K-30. Jayanti and Hewitt [18] employed CFD techniques to calculate the flow field and heat transfer through a wavy liquid film in order to study the heat transfer and hydrodynamics in a thin-film flow. Meanwhile, Del Carlo et al. [19] established a straightforward model to assess the efficiency of mass transfer and dynamics in distillation columns. Banerjee et al. [20] assessed the heat and mass transfer that takes place on the surface of liquid ethanol using a computer

model. Haroun et al. [21] explored the influence of liquid flow rate and structured packing geometry on both liquid hold-up and mass transfer. In addition, the authors of Turgut and Coban [22], Wen et al. [23], and Xu et al. [24] conducted their numerical and experimental research on the liquid desiccant dehumidifier to examine the performance of a liquid falling film dehumidifier. Meanwhile, Wen and Lu [25] studied film shrinkage form and vapor condensation in internally cooled LDD, and Luo et al. [26] reported a fin-tube type internally cooled LDD both for experimental and CFD simulation. Again Qi and Lu [27] optimized a survey of an internally cooled/heated LDAC system. Qi et al. [28, 29] investigated the liquid contact angle and its influence on the LDD system and the wetted area and film thickness for the falling film LDR system, respectively. Bouzenada et al. [30] and Dong et al. [31] reported the dehumidification performance of the LDAC system and enhanced the dehumidification performance by TiO<sub>2</sub> super-hydrophilic coating on the plate of LDD, whereas Lu et al. [32] investigated the dynamic characteristics of the counter-current flow for LDD system.

Das et al. [33] assessed the effectiveness of surface-modified LiCl and CaCl<sub>2</sub>-based falling film dehumidification in a cooling system, while another study by Das et al. [34] explored the performance of liquid desiccant absorber for the corrugated triangular structure where the volume of fraction (VOF) approach is utilized to monitor the interface of gas-liquid and penetration theorem is employed to estimate the mass transfer coefficients. Lyu et al. [35] demonstrated the effects of air parameters such as air velocity, flow pattern, and pressure on LiCl-H<sub>2</sub>O flow behavior in a liquid desiccant system. Das et al. [36] reported a numerical model of an LDD system with the trapezoidal baffled surface that involves a conjugate heat-mass interaction in a 2-D transient, multiphase, multi-component system. Du et al. [37] developed an internally cooled dehumidifier by incorporating the corrugated fins into the system to seek more contact area and enhance the system's efficiency as well as compatibility. The temperature adjustments are optimized as per recommendation and the reliability is ensured by the excellent precision of the correlation, which is within  $\pm 25$  percent. In another study, Du et al. [38] analyzed the thermal effect of a flat tube with many channels and corrugated fins that are internally cooled with its strengthening mechanism. Gao and Lu [39] reported a parametric analysis of a membrane distillation LDR with heat/moisture recovery and potable water production. Khan et al. [40] studied heat and mass transfer in adiabatic regeneration of LiCl desiccant on vertical and modified polypropylene surfaces under full and partial wetting conditions. Peng et al. [41] used CFD with the RNG  $k-\epsilon$  model and a user-defined function to optimize a falling film dehumidifier by varying the number and width ratio of rectangular cylinders. Moreover, Rokhman et al. [42] conducted a CFD analysis to model and enhance dehumidification performance in

a three-dimensional evaporative cooling-type film dehumidifier. Zhao et al. [43] reported also a CFD analysis to survey the performance of falling film LDD dehumidifier over sinusoidal and corrugated plates. Based on the findings, a mass transfer correlation was established and the effects of plate shape, moist air psychrometric characteristics, and solution parameters were examined. Zhou et al. [44] developed a mathematical model to describe the falling film flow on the surface of the flat-finned tube heat exchanger in a closed-type heat source tower, where the interface characteristics of gas-liquid falling film flow consider the interface forces. Meanwhile Mondal et al. [45, 46] revealed the results of an experimental study on a small-scale vapor absorption cooling system and bend tube water to the air heat exchanger, while Mondal and Islam [47] investigated the intermittent ammonia absorption refrigeration system. To aid in selecting the most suitable refrigerant for future air conditioning and refrigeration systems, Mondal et al. [48–52] measured the heat transfer coefficients and transport properties of various low GWP refrigerants. Moreover, Das et al. [53] conducted a thermodynamic study of a dual cascading vapor compression cycle and an organic Rankine cycle driven by solar energy, where two cases of power generation and cooling effects are studied.

Several studies have shown this by combining vapor compression (VC) technology with liquid desiccant systems. Kumar et al. [54] reported a review of the progressive study for hybrid cooling in liquid desiccant-vapor compression systems, using a dehumidification method can provide a reasonable degree of cooling while saving 40–80% on energy. Zhao et al. [55] presented an overview of mass, heat, and hydrodynamic transfer in falling film evaporation, absorption, cooling, and dehumidification in order to investigate the effect mechanism of a gas stream and obtain precise profiles of flow, temperature, and concentration. Fahad et al. [56] investigated a survey of materials, systems, and applications for the progressions in liquid desiccant technologies. Koronaki et al. [57] conducted a study of an adiabatic dehumidifier with various liquid desiccants. Park et al. [58] demonstrated an energy benefit of a hybrid LDD and evaporative cooling-assisted system for building air conditioning, whereas Mohammad et al. [59] detailed an examination of an integrated vapor compression system-based LDD system for use in buildings. Moreover, Rafique et al. [60] presented a review work on the regenerative method of solid/liquid desiccant system and its application in the drying system, while Jani et al. [61] reported a review of liquid desiccant dehumidifiers where summarized the performance parameters have been made to analyze the system performance. Meanwhile, Misha et al. [62] reported a review on liquid desiccant dehumidification-assisted cooling systems.

From the debate mentioned earlier, some studies were performed with smooth and rough vertical plates for LDD. However, there is an issue of considering the plate at some

angle with the vertical axis. To date, little to no research has been done taking the angle of inclination of the plate at any angle. There is no need for the plate or channel of moist air to be always vertical. Therefore, this study aimed to analyze the desiccant dehumidifier performance in three configurations: vertical smooth, vertical rough, and inclined rough plates, respectively, where LiCl is used as a liquid desiccant to absorb moisture from the air. The angle of inclination was considered and vapor absorption simulation was done in inclined plate LDD. In the test section, the desiccant will flow downwards for gravitational force and airflow will be set opposite to the desiccant flow from vertically downward to upward. Then, the amount of moisture collected from the air was investigated by the simulation using ANSYS workbench 2020 R1. The investigation was also carried out by placing the plates inclined and then the mass transfer rate was observed and compared to the vertical plate observations.

## METHODOLOGY

Wen et al. [3] specifically developed an experimental bench to find the impacts of various parameters on the dehumidification features, and Lu and Lu [2] then provided numerical justification for this work. Figure 1 exhibits the schematic diagram of the test bench of this experiment. It had three loops, each of which was identified by a different color of arrow. They were made up of three loops: one for liquid desiccant, one for processing air, and one for cooling water. All loops were stuffed with neoprene foam on the surfaces for thermal isolation. The entire setup was built in a lab with the ability to maintain a relatively constant level of moisture and temperature. To mitigate corrosion from LiCl

solution and to improve dehumidification efficiency, stainless steel 316L, known for its excellent corrosion resistance, was chosen for the plate dehumidifier [3]. In this study, the material of different plate configurations is considered as stainless steel. The vertical and inclined smooth and rough plates of falling film LDD are optimized in the main test section which is presented in Figure 2. In the main test section, the LiCl solution of different concentrations is used as a working substance for the various plate geometries: vertical smooth, vertical rough, and inclined rough.

## Physical Model

The three different forms of plate configurations for falling film liquid desiccant dehumidifiers are simplified and depicted in Figure 2. One is vertical smooth, one is a rough vertical plate and another is an inclined rough plate, respectively. The moist air flows in a counter-current direction at the bottom, whereas the desiccant film falls from top to bottom. The liquid desiccant dehumidifier (LDD) has a length of 150 mm and a width of 10 mm, with a width of 2 mm at the top of the liquid desiccant inlet, where the liquid desiccant is supplied through the length of the dehumidifier. In the vertical smooth plate shown in Figure 2(a), the liquid desiccant solution is flown along a 150 mm long plate, whereas the vertical rough plate shown in Figure 2(b) is spaced 10 mm apart and 1 mm in height. To enhance heat transfer, the vertical rough plate casing features ribs that are 1 mm high and 10 mm apart; the rib pitch-to-height ratio is regarded as 10. Both the first rib and the outlet of liquid desiccant are 30 mm apart, as is the distance between the liquid desiccant input and the last rib. Figure 2(c) represents the geometry of the inclined rough plate. The inclination of the rough plate is  $30^\circ$  from the vertical axis or  $60^\circ$  from the

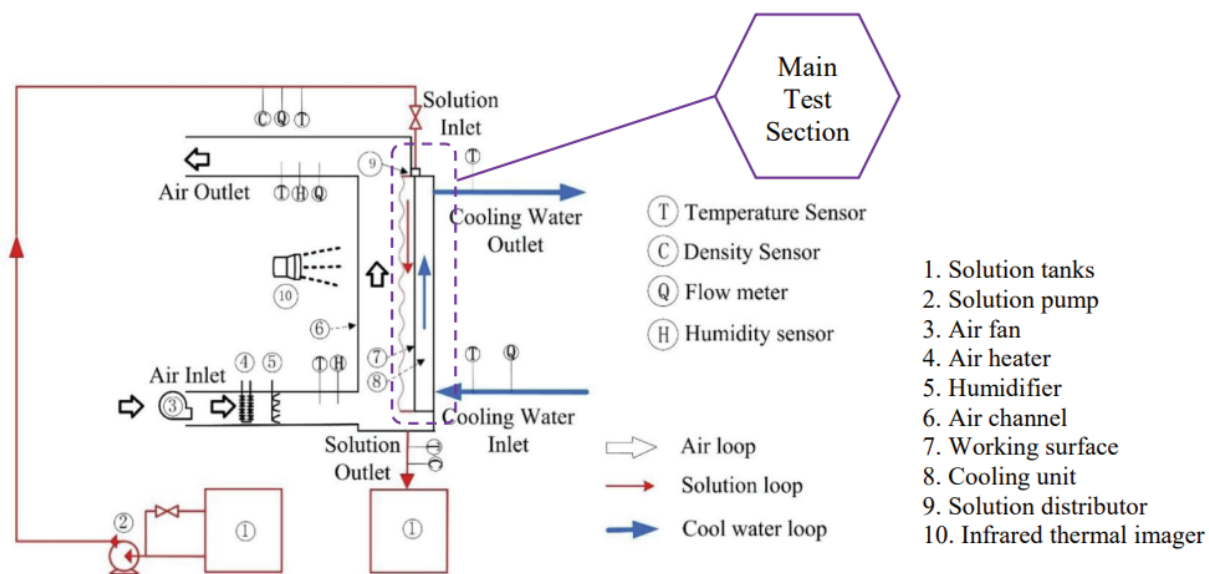


**Figure 1.** Illustration of experimental falling film dehumidifier of vertical plates of LDD. [From Wen et al. [3], with permission from Elsevier, License Number: 5880760582683].

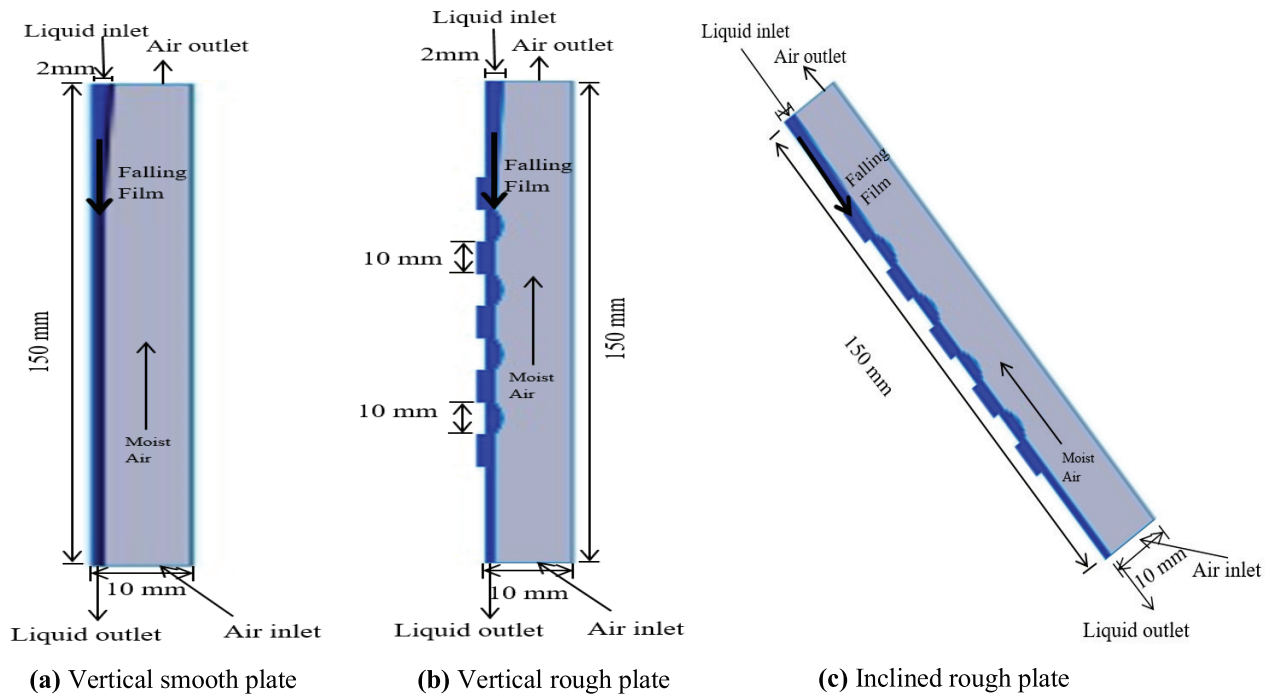


**Figure 2.** Geometry of simplified falling film dehumidifiers (a) vertical smooth, (b) vertical rough, and (c) inclined rough plates of LDD.

horizontal axis, rather all other specifications are the same as the vertical rough plate. Moreover, Figure 3 depicts the flow chart of the proposed model wherein the entire steps have been incorporated to gain insights into the work. The concentration of LiCl solution is considered as 30%, 33%, 36%, 40%, and 44%, respectively, for the justification of the influence of various concentrations of LiCl solution. While the inlet air velocity is considered as 0.5, 1.0, 1.5, and 2.0 m/s, respectively.

**Formation of the Problem**

In the current study, simulations have been conducted using ANSYS workbench 2020 R1. The choice of a pressure-based solver was made because the flow of both moist air and desiccant is incompressible with the constant density. The energy equation has also allowed us to understand the heat transfer mechanisms involved in the system. It is found that the liquid-dropping film is somewhat turbulent, while the airflow is turbulent overall. To model the gas-liquid flow, various turbulence models have been used, including the conventional k-ε model, RNG k-ε model, and Reynolds stress model, based on the work done by Banerjee and Isaac [63]. This simulation methodology has proved effective in analyzing the behavior of the moist air and desiccant flows and could be useful in designing and optimizing similar systems in the future.

The modeling of the gas-liquid interface has been solved accurately using the volume of fraction (VOF) model. This VOF model is utilized in this study to track the free surface

of the two-phase flow. The piecewise linear interface calculation (PLIC) technique, in particular, makes the VOF model flexible and efficient [1, 2]. The mass and momentum conservation equations for the gas-liquid two-phase system rely on the volume fractions of the gas and liquid. Nonetheless, the density ( $\rho$ ) and viscosity ( $\mu$ ) characteristics for every computational cell are displayed as follows:

$$\rho = \alpha_l \rho_l + \alpha_g \rho_g \tag{1}$$

$$\mu = \alpha_l \mu_l + \alpha_g \mu_g \tag{2}$$

Where,  $\alpha_g$  and  $\alpha_l$  are the gas and liquid volume fractions, respectively. Again,  $\rho_g$  and  $\rho_l$  present the gas and liquid phase's density, respectively. The fluid computational cell is defined as  $q_{th}$  for  $\alpha_q = 1$  while  $q_{th}$  for  $\alpha_q = 0$  and  $0 < \alpha_q < 1$  for empty fluid indicating that the cell has contact between the  $q_{th}$  fluid and other fluids. So, the total volume fraction of liquid-gas adds up to 1 which is as follows:

$$\alpha_l + \alpha_g = 1 \tag{3}$$

Therefore, the equations [1, 2] are to be solved for the volume fraction in order to track the gas and liquid interface and written as:

$$\frac{\partial \alpha_{l/g}}{\partial t} + u \cdot \nabla \alpha_{l/g} = 0 \tag{4}$$

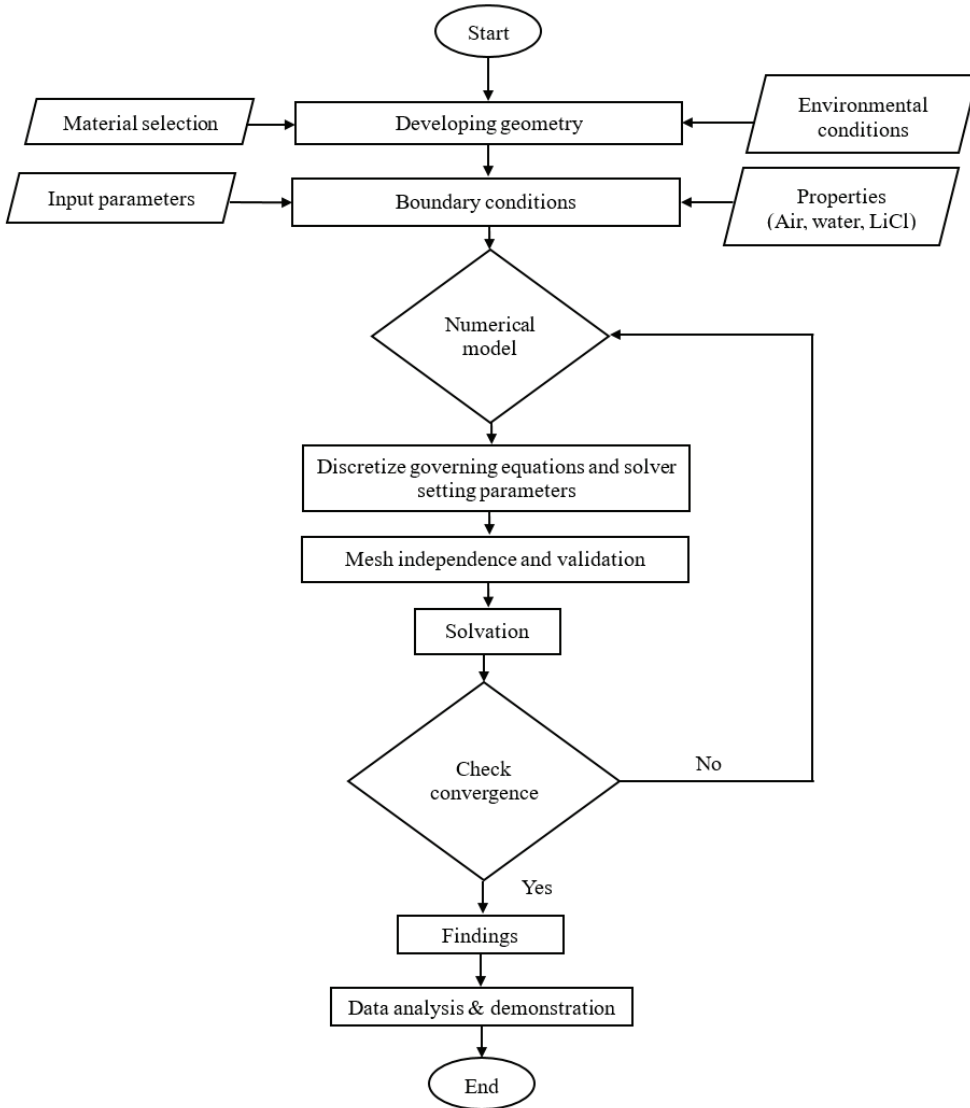


Figure 3. Flow chart of the proposed model.

Both the air flow and the liquid-dropping film exhibit some degree of turbulent behavior. Banerjee and Isaac [63] projected gas-liquid flow using several turbulence models, such as the RNG k-ε model and the conventional k-ε model. Comparing the RNG k-ε model with the experimental measurement yielded superior results than other turbulence models in terms of accuracy. Thus, the RNG k-ε turbulence model was used in this investigation. The following are the details of the governing equations used in the study to describe how moist air passes through a liquid desiccant, including the VOF model, energy, momentum, species, and turbulence equations [1, 2, 63].

Thus, the continuity equation is written as follows:

$$\frac{\partial}{\partial t} \rho + \nabla \cdot (\rho u) = 0 \tag{5}$$

The momentum equation is written as follows:

$$\frac{\partial}{\partial t} \rho + \nabla \cdot (\rho u u) = -\nabla P + \nabla \cdot (\mu (\nabla \mu + \nabla u T)) + \rho g + F \tag{6}$$

The energy equation is written as follows:

$$\frac{\partial}{\partial t} (\rho E) + \nabla \cdot (u (\rho E + P)) = \nabla \cdot (k_{eff} \nabla T - \sum h_k J_k) + S_E \tag{7}$$

Where,  $\rho$  and  $u$  are the fluid density and velocity, respectively. While  $k_{eff}$  is the effective thermal conductivity,  $F$  is the momentum source term and  $S_E$  is the energy source term, respectively. To calculate the turbulent kinetic energy and its rate of dissipation, the transport equation is represented as follows:

$$\frac{\partial}{\partial t}(\rho k) + \frac{\partial}{\partial x_i}(\rho k \mu_i) = \frac{\partial}{\partial x_j} \left( \alpha_k \mu_{eff} \frac{\partial k}{\partial x_j} \right) + G_k + G_b - \rho \varepsilon - Y_M + S_E \quad (8)$$

Where,  $G_k$  represents the generation of turbulence kinetic energy due to mean velocity gradients, while  $G_b$  represents the generation of turbulence kinetic energy due to buoyancy. The turbulence dissipation rate transport equation can be expressed as follows:

$$\frac{\partial}{\partial t}(\rho \varepsilon) + \frac{\partial}{\partial x_i}(\rho \varepsilon \mu_i) = \frac{\partial}{\partial x_j} \left( \alpha_\varepsilon \mu_{eff} \frac{\partial \varepsilon}{\partial x_j} \right) + C_{\varepsilon 1} \frac{\varepsilon}{k} (G_k + G_{3\varepsilon} G_b) - C_{\varepsilon 2} \frac{\varepsilon^2}{k} + R_\varepsilon + S_\varepsilon \quad (9)$$

Where  $\varepsilon$  is the turbulence dissipation rate by considering  $C_{\varepsilon 1} = 1.42$ ,  $C_{\varepsilon 2} = 1.68$ , and  $\alpha_k = 1.393$ . The following is an expression for the transport equation:

$$\frac{\partial}{\partial t}(\alpha_q \rho_q Y_{k,q}) + \nabla \cdot (\alpha_q \rho_q u Y_{k,q} - \alpha_q \Gamma_{k,q} \nabla Y_{k,q}) = S_{lg,k} \quad (10)$$

Where,  $Y_{k,q}$  denotes the  $k$  component's mass fraction of  $q^{\text{th}}$  phase, and  $S_{lg,k}$  presents the source term of mass transfer. Again, the continuous surface tension model is to be used to explain the surface tension at the gas-liquid free surface, and it looks like this:

$$F_{ST} = \sigma_{ij} \frac{\rho k_i \nabla \alpha_i}{(\rho_i + \rho_j)/2} \quad (11)$$

Where,  $\sigma_{i,j}$  represents the coefficient of surface tension. Moreover, the dynamic dehumidification process was examined by applying the mass transfer theory of penetration. It was not taken into account the mass transfer barrier at the gas-liquid contact [1, 2, 7]. The coefficient of overall mass transfer ( $M_g$ ) may be written as follows:

$$\frac{1}{M_g} = \frac{1}{h_{m,g}} + \frac{1}{\psi h_{m,l}} \quad (12)$$

Where,  $h_{m,g}$  and  $h_{m,l}$  are the gas and liquid phases' respective local mass transfer coefficients, while  $\psi$  is expressed as a function of temperature and concentration of liquid desiccant in the following way:

$$\psi = \alpha_0 + \alpha_1 T_s + \alpha_2 (T_s)^2 + \alpha_3 (T_s)^3 \quad (13)$$

According to the literature by Zhang et al. [7], the values of  $\alpha_i$  (where  $i = 0, 1, 2$ , and  $3$ ) are estimated and the coefficients of local mass transfer are calculated as follows:

$$h_{m,g} = 2 \sqrt{\frac{D_g}{\pi t_c}}, \quad h_{m,l} = 2 \sqrt{\frac{D_l}{\pi t_c}} \quad (14)$$

Where,  $D_g$  and  $D_l$  are the diffusion coefficients of the gas and liquid phases, respectively, at a certain contact time ( $t_c$ ). Again, the mass transfer source is estimated at a contact area of  $A$  by considering the bulk air humidity ratio ( $W_{g,b}$ ) and equilibrium air humidity ratio ( $W_{g,e}$ ) to the desiccant, respectively. Thus, the source of mass transfer ( $S_{lg,k}$ ) is written as follows:

$$S_{lg,k} = M_g (W_{g,b} - W_{g,e}) A \quad (15)$$

$$W_{g,e} = 0.622 \frac{P_{l,b}}{P_a - P_{l,b}} \quad (16)$$

Then, the mass transfer's latent heat is the energy source term ( $S_E$ ), which is shown as follows:

$$S_E = \sum_{k=0}^{m-1} S_{lg,k} H_{lg,k} \quad (17)$$

### Boundary Conditions and Setup

In this work, the numerical problem is solved using an ANSYS fluent pressure-based solver. The mass transfer mechanism is used at a constant rate of 50 mol/s. The LiCl solution mixture used consists of 30-44 % LiCl and 56-70 % water liquid, while the moist air consists of 1.6-2.4 % water vapor and 97.6-98.40 % air. The simulation utilizes a velocity inlet boundary at the air exit whereas the solution is an inlet and a pressure outlet boundary for the entry of the moist air and the exit of the solution. The plate is set as a wall boundary, and the right side of the moist air flow uses a symmetry boundary. The VOF model tracks the interface of the two-phase flow, incorporating surface tension effects within the interfacial forces considered in the simulation. To complete the simulation the following fluid flow assumptions are considered: (i) the flowing fluid is incompressible, (ii) the fluid is two-phase flow, (iii) the unsteady gas-liquid fluid flow conditions, (iv) the no-slip boundary condition, and (v) negligible body force. However, Table 1 lists the input parameters for this study, while Table 2 displays the properties of fluids. Once more, Table 3 lists the numerical setup along with the solver setting parameters.

**Table 1.** Input parameters for the simulation in this study

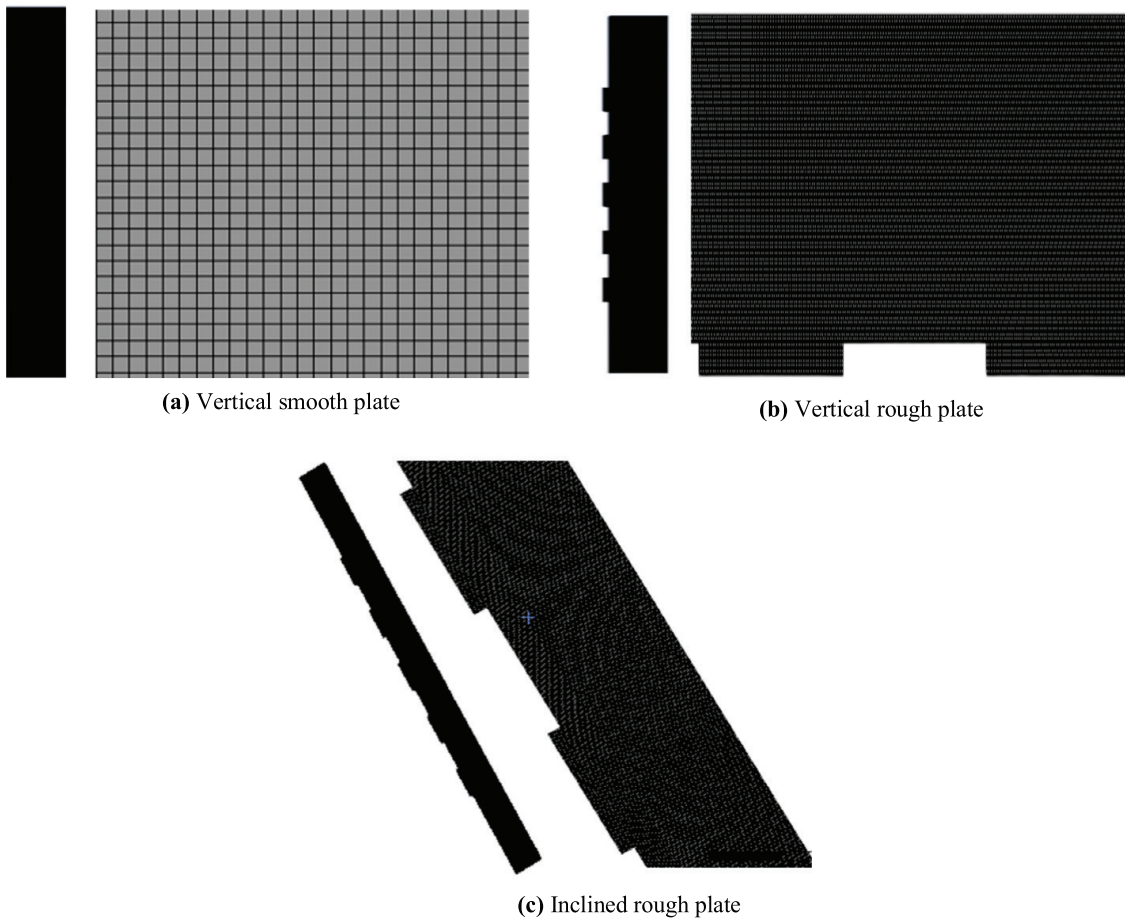
Plates	Solution Concentration (%)	Solution velocity (m/s)	Moist air velocity (m/s)	Inlet mass fraction of water vapor (%)	Surface tension coefficient (N/m)	Moist air inlet Temp. (K)	LiCl solution inlet Temp. (K)
Vertical Smooth	30-44	0.3	0.5-1.5	1.6-2.4	0.0893	303	298
Vertical Rough	30-44	0.3	0.5-1.5	1.6-2.4	0.0893		
Inclined Rough	30-44	0.3	0.5-1.5	1.6-2.4	0.0893		

**Table 2.** Properties of air, LiCl, and liquid & water vapor [64]

Parameter	Air	LiCl	Water	
			Liquid	Vapor
Density (kg/m <sup>3</sup> )	1.225	1180	998.2	0.5542
Specific Heat (J/kg.K)	1006.43	2933	4182	2014
Thermal Conductivity (W/m.K)	0.0242	0.42	0.6	0.0261
Viscosity (kg/m.s)	1.7894×10 <sup>-5</sup>	0.00359	0.001003	1.34×10 <sup>-05</sup>
Molecular Weight (kg/K mol)	28.966	42.394	18.0152	18.01534

**Table 3.** Numerical setup with solver setting parameters and solution methods

Parameter	Setup	Parameter	Setup
Solver Type	Pressure-based	Fluids	Air, LiCl, and liquid & vapor water
Time	Transient	Mesh	Face meshing with a quadrilateral element
Velocity	Absolute	Formulation	Explicit
Model	Volume of Fluid (VOF)	Pressure	PRESTO!
Phase	Multiphase (2)	Gradient	Least Squares Cell-Based
Viscous Model	Turbulent (RNG k- ε Model)	Pressure velocity coupling	SIMPLE

**Figure 4.** Illustration of the mesh geometry and structural grids of (a) vertical smooth, (b) vertical rough, and (c) inclined rough plates of LDD.

**Table 4.** Mesh information at various plate configurations of LDD

Information	Vertical smooth plate	Vertical rough plate	Inclined rough plate
Mesh element	182500	178520	160270
Orthogonal quality	0.99856	0.99759	0.99556
Aspect ratio	1.0096	1.0295	1.0393
Skewness	$4.27 \times 10^{-03}$	$5.1252 \times 10^{-02}$	$5.3119 \times 10^{-02}$

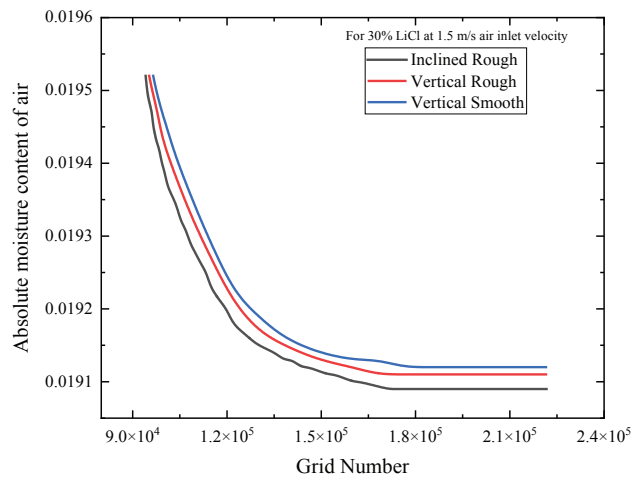


**Figure 5.** Grid independence test.

**Grids Independence and Validation**

The mesh independence test was carried out using a series of simulations for vertical smooth, vertical rough, and inclined rough plates. The commercial software ANSYS meshing was used to mesh the inclined and vertical plates. Better convergence and wall function were the goals behind the development of face meshing. The meshing with the quadrilateral element of the blunt body for the whole domain is shown in Figure 4. The mesh geometry and structural grids of the vertical smooth plates and the vertical rough plates are illustrated in Figures 4(a) and (b), respectively, while Figure 4(c) represents the mesh geometry and structural grids of the inclined rough plate where the inclination of the rough plate is 30° from the vertical axis or 60° from the horizontal axis.

Moreover, Figure 5 demonstrates the study carried out to investigate the impact of grid resolution on the simulation outcomes which is commonly known as grid independence. When the grid number exceeds 150270, there is no effect on the computational result of the absolute moisture content of air. Even though, the moisture content of the air passing through the LDD plates did not noticeably change with additional grid refining. As a result, the grid numbers 182500, 178520, and 160270 were adopted in this work for vertical smooth, vertical rough, and inclined rough plates,

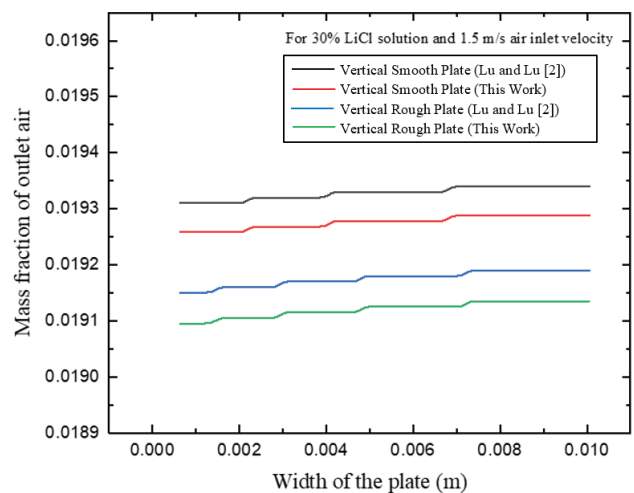


**Figure 6.** Variation of mass fraction of outlet air corresponding to the width of the plate.

respectively, while Table 4 shows the mesh information about the various plate configurations.

Figure 6 depicts the variation of mass fraction outlet air with respect to the width of vertical smooth and rough plates. From this figure, the mass fraction of outlet air is gradually increased along the plate width which indicates a similar trend to the findings by Lu and Lu [2]. The data suggest that the deviation in the graphs for smooth plates is around 2.5%, while for vertical rough plates, it is approximately 3.9%. By the way, the deviation of this work with Lu and Lu [2] is relatively small and it varies depending on the plate being analyzed. This implies that the deviation in the results is less pronounced in the case of smooth plates when compared to rough plates.

**RESULTS AND DISCUSSION**

In this study, the impact of air velocity on the mass transfer enrichment and temperature increments of LDD was numerically studied by ANSYS. The 30% LiCl solution is used as an absorbent and hence, the result section presents the findings, while the discussion section interprets and explains their meaning in the context of the research. Moreover, the LiCl solution’s mass concentration is taken into account as 30%, 33%, 36%, 40%, and 44%, respectively,

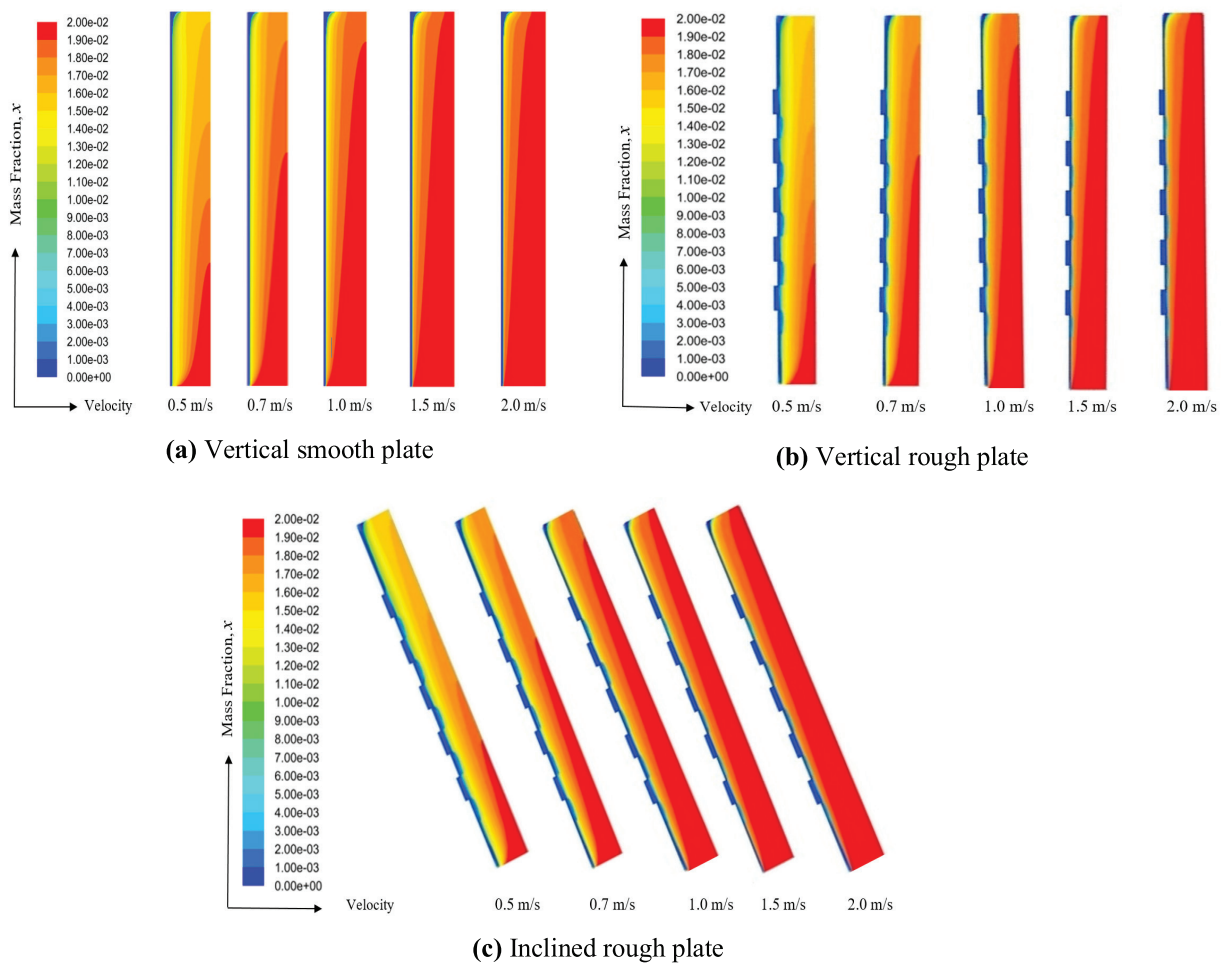
for the justification of the influence of various concentrations of LiCl solution. While the inlet air velocity is considered as 0.5, 1.0, 1.5, and 2.0 m s<sup>-1</sup>, respectively. This analysis was validated with the study of Lu and Lu [2], where the deviations are found 2.5% and 3.9% for vertical smooth and vertical rough plates, respectively, corresponding to the measurement of the mass fraction of outlet air. Overall, this simulation was effectively carried out for all the variabilities such as moisture content, outlet air temperature, and concentration of LiCl solution within the error limit of 6.75%.

### Influence of Air Velocity

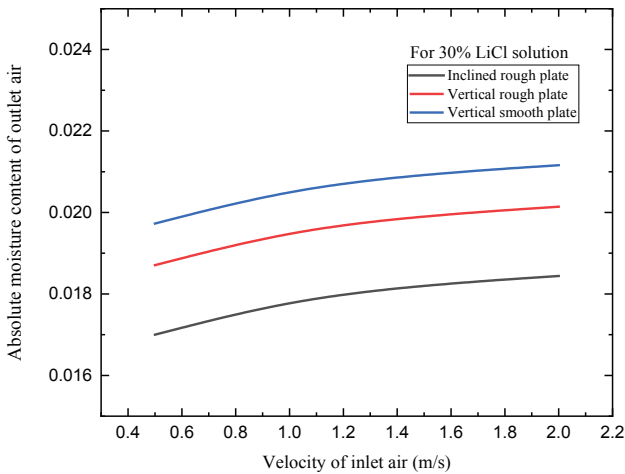
The research has been done to examine how air velocity affects LDD's mass transfer enhancement for the three geometries as the main test section (vertical smooth, vertical rough, and inclined rough plates). For this consequence, it is necessary to adjust the air velocity in practical dehumidification applications. However, Figure 7 shows the contours of the moist air mass fraction under various air inlet velocities for vertical smooth, vertical rough, and inclined rough plates, respectively. The red area denotes

the wet air, while the blue area is the liquid desiccant. It is noticed that the reduction in the air velocity leads to a significant decrease in the outlet mass fraction of water vapor from moist air. When the velocity of the incoming moist air is higher, the outlet air mass fraction increases, which suggests that the liquid LiCl solution cannot absorb enough moisture due to insufficient time.

As the velocity of inlet moist air increases in Figure 7(a), the outlet air mass fraction increases up to 2.1 % which indicates a decrease in water vapor absorption as the LiCl liquid solution did not get sufficient time to absorb moisture. This goes the same for the vertical rough plate up to 2 %, shown in Figure 7(b). But in the case of an inclined rough plate, the amount of mass fraction decreases which means an increase in water vapor absorption because of inclination and ribs the friction increases which is observed in the contour in Figure 7(c). It is seen that the red area is getting yellow from the red zone as air gradually goes upward. At the ribs, it is blue because there is no mass of water vapor at the boundary but it is getting greener at the contact surface with moist air.



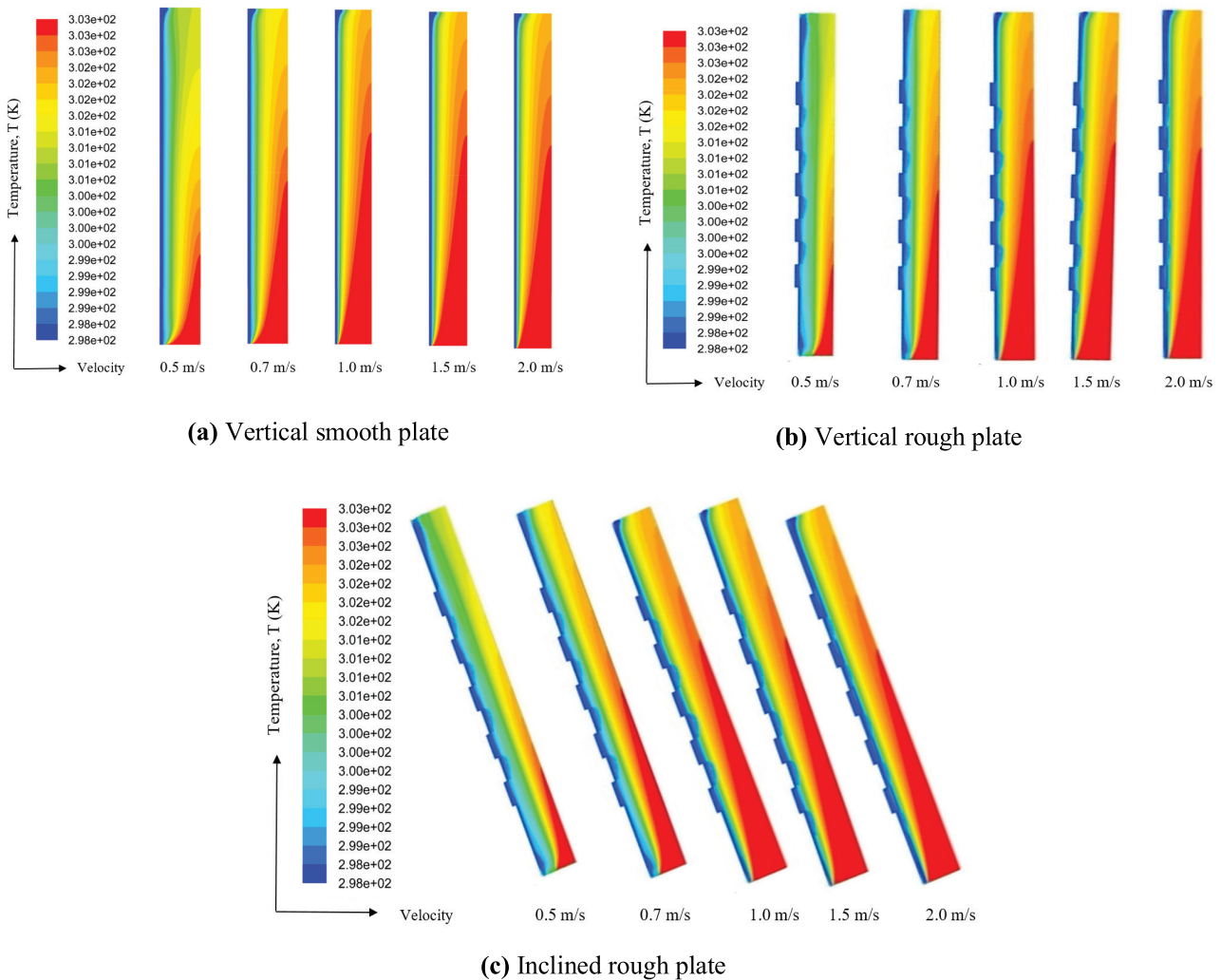
**Figure 7.** Contours of outlet air mass fraction under various air inlet velocities for (a) vertical smooth, (b) vertical rough, (c) inclined rough plates of LDD (for 30% LiCl solution).



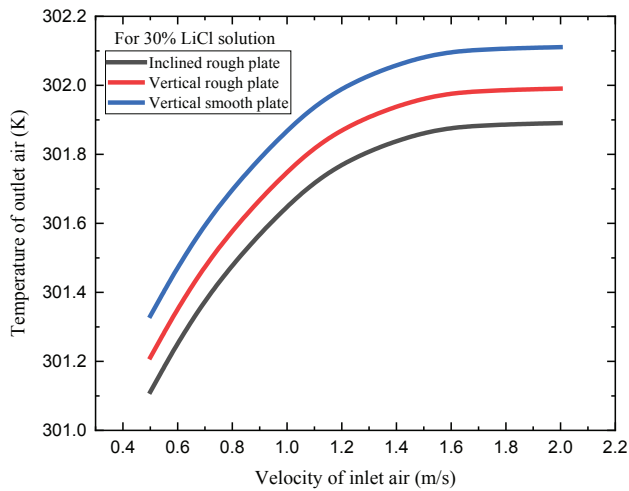
**Figure 8.** Outlet air mass fraction under various air inlet velocities.

Figure 8 describes the variation of absolute moisture content of air under various air inlet velocities with 30% LiCl solution that indicates the comparison of moisture absorption vertical smooth, vertical rough, and inclined rough plate. To put it simply, the outcomes show that as the velocity of incoming moist air rises, the ability of the liquid LiCl solution to absorb moisture decreases. This effect is seen in both vertical smooth and vertical rough plates. The absolute moisture contents of outlet air are recorded as the maximum of 2.1% and 2.0% for vertical smooth and rough plates, respectively. In the case of an inclined rough plate, the moist air mass fraction decreases, indicating an increase in water vapor absorption with an increase in the inlet air velocity. This is because the inclination and ribs increase friction, which helps to absorb more moisture. In this case, the absolute moisture content of outlet air is found a maximum of 1.8%.

Figure 9 shows the contours of outlet air temperature under various air inlet velocities for vertical smooth, vertical



**Figure 9.** Contours of air temperature under various air inlet velocities for (a) vertical smooth, (b) vertical rough, and (c) inclined rough plates of LDD (for 30% LiCl solution).



**Figure 10.** Variation of outlet air temperature under various air inlet velocities.

rough, and inclined rough plates, respectively. As the velocity of inlet moist air increases in Figure 9(a), the outlet air mass fraction increases indicating a decrease in water vapor absorption and hence, the temperature of the outlet air does not decrease much from inlet. As the velocity is increasing the red area is increasing because of the short time of absorption. This goes almost the same for vertical smooth and rough plates but slightly good findings are observed in the vertical rough plate shown in Figure 9(b). In an inclined rough plate shown in Figure 9(c), the amount of temperature decreases more than in vertical smooth and rough plates which means an increase in water vapor absorption due to the inclination and ribs, which create friction. When moist air flows that test section at 0.5 m/s in the upward direction into the vertical smooth, vertical rough, and inclined rough plate configurations, the minimum outlet air temperatures are recorded as 301.3 K, 301.2 K, and 301.1 K, while maximum temperatures are found as 302.14 K, 302.0 K, and 301.85 K at a moist air velocity of 2.0 m/s, respectively.

Figure 10 illustrates the variation of air temperature under various air inlet velocities of vertical and inclined plates of LDD, respectively. The temperature of outlet air rapidly increases with raising the inlet air velocity until 1.1 m/s and then gradually increases along the vertical and inclined plates. The rapid increase of outlet air temperature indicates less water vapor absorption and hence, the temperature of outlet air for the vertical smooth plate is greater than the rough plate. Moreover, in the inclined rough plate, the temperature of outlet air is quite smaller than the vertical smooth and vertical rough plate. So, inclination is quite efficient for dehumidification purposes.

#### Influence of the Varying Lengths of the LDD Plates

The temperature of air initially increases in the inlet section and then slightly decreases along the plate length when passing the outlet section by variation as the inlet air

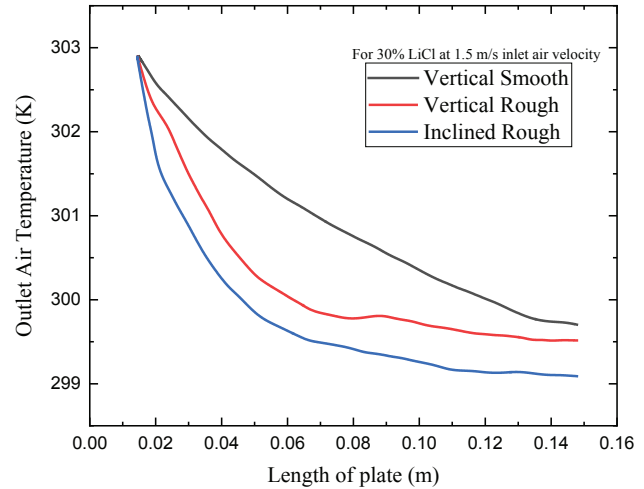


**Figure 11.** Variation of outlet air temperature along the length of the plates.

velocity increases. The change in air temperature is affected by two factors. Initially, the desiccant cools the air through sensible heat exchange because its temperature is lower than the air. Subsequently, as water condenses from the air, latent heat is released, raising the air temperature. The interplay between these two processes results in the observed fluctuations in the outlet air temperature.

Figure 11 shows the temperature distribution of outlet air along the length of the plates of LDD. The length of plates (150 mm) from bottom to top, the temperature of the moist air is decreasing because the water vapor is absorbed by LiCl solution. Along the plate length, the outlet air temperature decreasing is quite less for the vertical smooth plate. But it is quite higher in vertical rough plates and highest in inclined rough plates. The outlet air temperatures were measured through the plate width by considering 30% LiCl solution and 1.5 m/s moist air inlet velocity. The maximum air temperature was measured at 302.8 K for the plate length of 0.02 m, while the minimum temperatures were recorded as 299.8 K, 299.5 K, and 299.15 K at the plate length of 0.15 m for vertical smooth, vertical rough, and inclined rough plate configurations, respectively.

Figure 12 interprets the temperature distribution of LiCl solution along the length (150 mm) of the plates of LDD. The temperature is going upward as the liquid LiCl desiccant is falling down from the top of the plates. Because of the absorption of moisture from the air, the temperature rises as comparatively warm air releases heat and liquid desiccant absorbs it. The trend is quite similar for all cases, but the temperature rise is less in the case of the inclined rough plate. Because of inclination, the absorption is more and so the temperature rise is less. The minimum temperature of LiCl solution was measured at 298 K, while the maximum temperatures were recorded as 302.5 K, 302.05 K, and 301.14 K at the plate length of 0.15 m for vertical smooth, vertical rough, and inclined rough plate configurations, respectively.

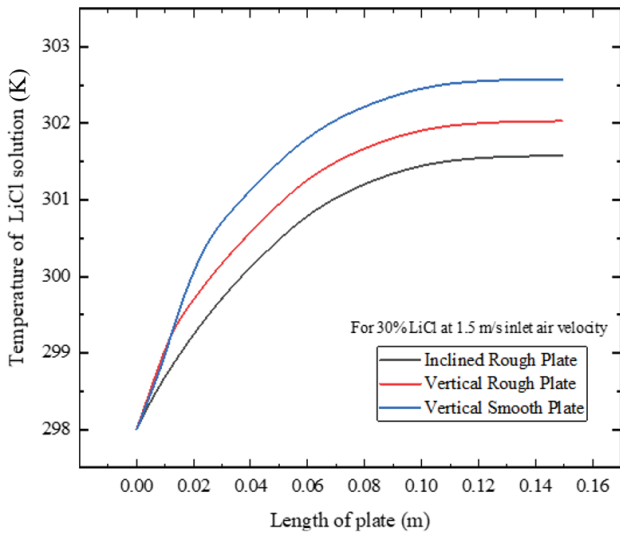


**Figure 12.** Variation of the temperature of LiCl solution along the length of the plates.

**Impact of Water Concentration of Inlet Air**

The outlet air mass fraction of the different plates is significantly influenced by the entrance air vapor percentage. Figure 13 shows the contours of the outlet air mass fraction under various inlet air vapor fractions for the vertical smooth & rough and inclined rough plates of LDD. The mass fraction of outlet air increases with increasing the inlet air vapor fraction along the plate length. The amount of water vapor absorption decreases with the increase of vapor percentage in inlet moist air. Figure 13(b) shows relatively good results for the vertical rough plate to the water absorption indicating less moisture content of outlet air than the vertical smooth plate from the incoming moist air to the LiCl solution. However, the moisture content of outlet air for the vertical rough plate increased instead of decreasing trend than the vertical smooth plate after the inlet air vapor quality of 0.018. Moreover, in an inclined rough plate shown in Figure 13(c), the friction increases due to the inclination, which is responsible for increasing the contact

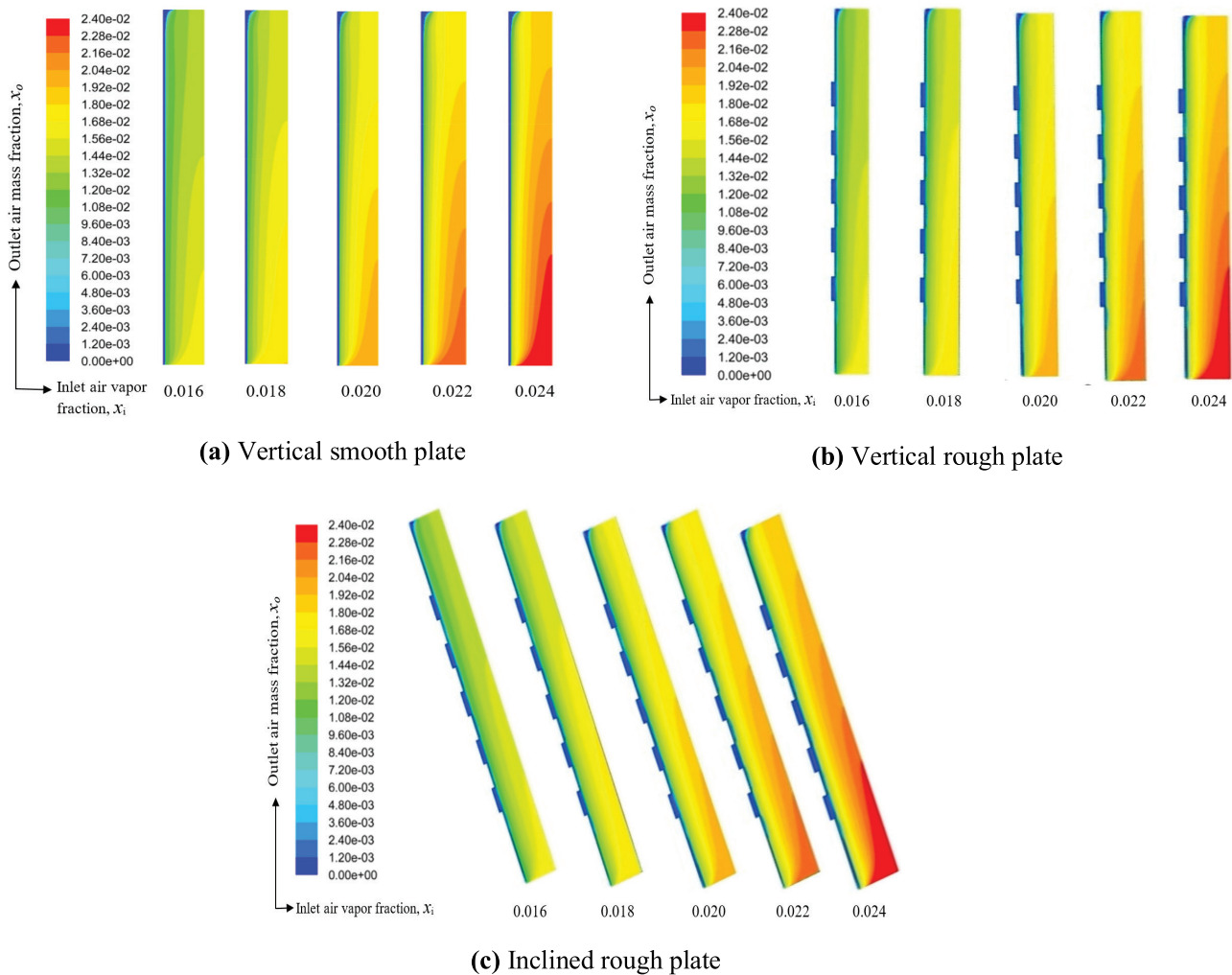


**Figure 13.** Contours of outlet air mass fraction under various inlet air vapor fractions for (a) vertical smooth, (b) vertical rough, and (c) inclined rough plates of LDD (for 30% LiCl solution).

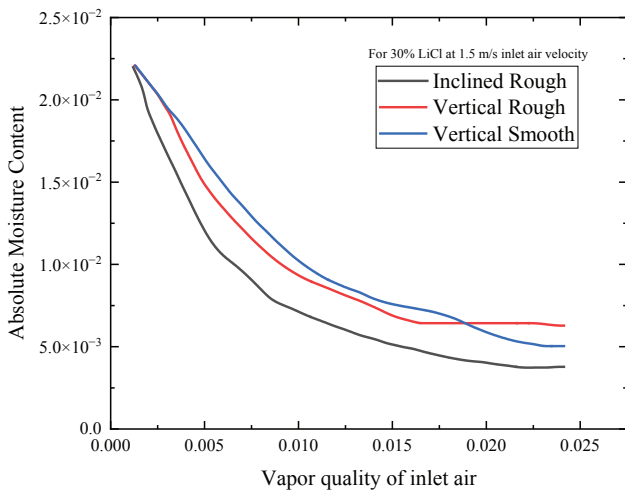


**Figure 14.** Outlet air moisture content in terms of inlet air vapor quality.

time and absorption rate. This leads to an increase in the absorption of water vapor despite an increase in the percentage of vapor in the inlet air. Therefore, the red area represents the absorption capacity of the inclined rough plate, which is significantly reduced compared to vertical smooth and rough plates.

Figure 14 reveals the comparison of water vapor absorption ability among vertical smooth, vertical rough, and inclined rough plates. It describes that a rise in the percentage of water vapor in incoming air results in a corresponding increase in the moisture content of outlet air. This indicates that the ability of the air to absorb water vapor decreased the mass fraction of outlet air by increasing the incoming moist air. Among all types of plates, inclined rough plates perform quite well because of the increased friction created by the inclination and ribs. That is why the absolute moisture content line of an inclined rough plate in the figure is at the bottom compared to the vertical smooth and rough plates. In summary, in an inclined rough plate, the absorption of water vapor is higher even when the percentage of vapor in the inlet air is increased.

**Influence of Various Concentrations of LiCl Solution**

The LiCl solution’s mass concentration is considered as 30%, 33%, 36%, 40%, and 44%, respectively. The inlet air velocity is 0.5, 1.0, 1.5, and 2.0 m/s, respectively. The fluctuation of the exit air mass fraction for various geometries under varied air inlet velocities is displayed in Figure 15. The outlet mass fraction is quite less when the smoothness of the plate decreases in the vertical rough plate than in the vertical smooth plate. While smoothness further decreases in the inclined rough plate, the water vapor absorption is found to a greater extent. Moreover, the velocity of inlet air increases then the moisture content in outlet air increases which indicates that vapor absorption quality decreases with an increase in velocity as the contact time between desiccant solution

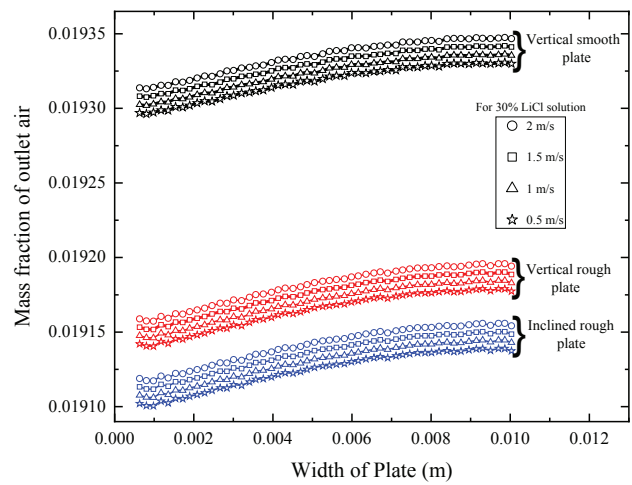


**Figure 15.** Outlet air mass fraction for different geometries under various air inlet velocities.

and moist air decreases. The trend of outcomes found by this work for the vertical smooth and rough plates of falling film LDD is almost similar to Lu and Lu [2].

Figure 16 demonstrates the effect of various LiCl solutions on outlet air mass fraction along the width of the inclined rough plate at 2 m/s air velocity. The mass concentration of the LiCl solution has been considered as 30%, 33%, 36%, 40%, and 44% respectively. Its ability to dehumidify is greatly influenced by the concentration of the liquid desiccant that is added. When the concentration of the entering liquid LiCl solution increases then the mass fraction of outlet air decreases which indicates the improvements in the liquid film’s ability to absorb water vapor from the incoming moist air. The mass fraction of the outlet air decreases which means water vapor absorption is increasing

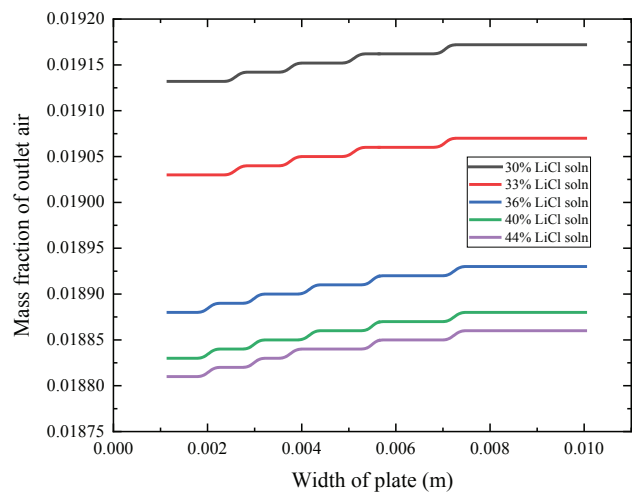


**Figure 16.** Outlet air mass fraction along the width of the inclined rough plate for various LiCl concentrations at velocity 2 m/s.

by increasing the concentration of LiCl solutions. But this limit is 30 to 40% because further, this limit water vapor absorption by LiCl solution does not increase significantly. An increased amount of concentration of LiCl absorbs the increased amount of vapor from moist air.

## CONCLUSION

This study sheds light on the importance of plate configurations in liquid desiccant dehumidifiers and their impact on the performance of dehumidification and gas-liquid flow. The findings highlight the significant role of inclined rough plates in enhancing dehumidification effectiveness by promoting increased water vapor absorption. The CFD simulation using the RNG k- $\epsilon$  turbulence model effectively predicted the dehumidification performance of a falling film LDD with various plate configurations under unsteady gas-liquid flow conditions. The key findings of this work are as follows:

- Increased inlet air velocity results in higher outlet air mass fractions, indicating reduced water vapor absorption due to insufficient time for the moist air and LiCl solution to come into contact.
- Among the plate configurations, the inclined rough plate significantly enhances dehumidification efficiency by generating liquid film waves and increasing the contact time, leading to a greater reduction in the outlet mass fraction of water vapor.
- In the inclined rough plate, it is noticed that the dehumidification enhancement goes up to 10.8% compared to the use of a smooth plate, particularly when the inlet air velocity is 1.5m/s.
- Higher inlet desiccant concentrations improve water vapor absorption, with an optimal range identified between 30% to 40% LiCl concentration. The study outcomes specify that the efficiency of enrichment remains consistent even with solution concentrations exceeding 36%, while the benefits may level off beyond a certain point.
- The inclined rough plate configuration consistently showed superior performance compared to vertical smooth and rough plates, making it the most effective design for improving dehumidification in LDD systems.

This research highlights the importance of factors like inlet desiccant concentration and air velocity in optimizing falling film liquid desiccant systems for dehumidification. Moving forward, further exploration and experimentation in this area can lead to advancements in liquid desiccant technology, ultimately contributing to energy savings and improved indoor air quality in various applications. By identifying these key factors and their effects, this research provides valuable insights into the design and operation of efficient and sustainable dehumidification systems.

## NOMENCLATURE

$D$	Coefficient of diffusion, $m^2/s$
$E$	Energy, J/kg
$F$	Source term momentum, $N/m^3$
$G_k$	Kinetic energy of turbulence produced by mean velocity gradients, $kg/(m \cdot s^3)$
$G_b$	Buoyancy-induced kinetic energy creation of turbulence, $kg/(m \cdot s^3)$
$g$	Gravitational acceleration, $m/s^2$
$h$	Enthalpy, J/kg
$h_m$	Coefficient of local mass transfer, $kg/(m^2 \cdot s)$
$H_{lg}$	Latent evaporation heat, J/kg
$J$	Mass flux, $kg/(m^3 \cdot s)$
$k$	Thermal conductivity, $W/(m \cdot K)$
$l$	Distance of liquid flow, m
$M_g$	Local total mass transfer coefficient, $kg/(m^2 \cdot s)$
$P$	Pressure, Pa
$P_a$	Atmospheric pressure, Pa
$P_{l,b}$	The bulk desiccant solution's partial vapor pressure, Pa
$S_{i,g}$	Source of mass transfer at phase interface, $kg/m^3$
$S_E$	Source term energy, $W/m^3$
$R_\epsilon$	Additional term, $kg/(m \cdot s^3)$
$t$	Time, s
$t_c$	Contact time, s
$T$	Temperature, K
$W_{g,b}$	Bulk air humidity ratio, kg/kg
$W_{g,e}$	Air humidity ratio in equilibrium with desiccant solution, kg/kg

### Greek symbols

$\alpha$	Volume fraction
$\mu$	Dynamic viscosity, $kg/(m \cdot s)$
$\psi$	Concentration ratio
$\rho$	Density, $kg/m^3$
$\epsilon$	Turbulence energy dissipation rate
$\sigma_{ij}$	Coefficient of surface tension, $kg/m^3$

### Subscripts

$a$	Air
$eff$	Effective
$g$	Gas phase
$l$	Liquid phase
$s$	Solution
$i,j$	Indication of the coordinate axis

## AUTHORSHIP CONTRIBUTIONS

**Md. Tamzid Shaharier (M. T. Shaharier):** Conceptualization, methodology, investigation, data acquisition, analysis, writing original draft, and editing manuscript.

**Dipayan Mondal (D. Mondal):** Conceptualization, methodology, investigation, data acquisition, analyzing and interpreting the data, writing, review and editing, discussion, supervising.

**Md. Abdul Hasib (M. A. Hasib):** Analyzing and interpreting the data, reviewing and editing, and writing.

**Md. Ashraful Islam (M. A. Islam):** Reviewing editing, and writing of reviewer response.

## DATA AVAILABILITY STATEMENT

Data will be available upon reasonable request from the corresponding author.

## CONFLICT OF INTEREST

The authors declared no conflicts of interest associated with this publication, and there had been no significant financial support for this work that could have influenced its outcome.

## ETHICS

There are no ethical issues with the publication of this manuscript.

## REFERENCES

- [1] Luo Y, Yang H, Lu L. Liquid desiccant dehumidifier: Development of a new performance prediction model based on CFD. *Int J Heat Mass Transf* 2014;69:408-416. [\[CrossRef\]](#)
- [2] Lu H, Lu L. CFD simulation of liquid desiccant dehumidifier performance with smooth and rough plates. *Int J Refrig* 2021;124:1-12. [\[CrossRef\]](#)
- [3] Wen T, Lu L, Dong C. Enhancing the dehumidification performance of LiCl solution with surfactant PVP-K30. *Energy Build* 2018;171:183-195. [\[CrossRef\]](#)
- [4] Liu XH, Jiang Y. Handling zone dividing method in packed bed liquid desiccant dehumidification/regeneration process. *Energy Conver Manage* 2009;50:3024-3034. [\[CrossRef\]](#)
- [5] Zhang LZ. Energy performance of independent air dehumidification systems with energy recovery measures. *Energy* 2006;31:1228-1242. [\[CrossRef\]](#)
- [6] Zhang F, Zhang Z, Geng J. Study on shrinkage characteristics of heated falling liquid films. *AIChE J* 2005;51:2899-2907. [\[CrossRef\]](#)
- [7] Zhang L, Hihara E, Matsuoka F, Dang C. Experimental analysis of mass transfer in adiabatic structured packing dehumidifier/regenerator with liquid desiccant. *Int J Heat Mass Transf* 2010;53:2856-2863. [\[CrossRef\]](#)
- [8] Das RS, Jain S. Experimental investigations on a solar assisted liquid desiccant cooling system with indirect contact dehumidifier. *Sol Energy* 2017;153:289-300. [\[CrossRef\]](#)
- [9] Zhang L, Liu X, Jiang J, Jiang Y. Exergy calculation and analysis of a dehumidification system using liquid desiccant. *Energy Build* 2014;69:318-328. [\[CrossRef\]](#)
- [10] Chen Y, Yin Y, Zhang X. Performance analysis of a hybrid air-conditioning system dehumidified by liquid desiccant with low temperature and low concentration. *Energy Build* 2014;77:91-102. [\[CrossRef\]](#)
- [11] Stevens DI, Braun JE, Klein SA. An effectiveness model of liquid-desiccant system heat/mass exchangers. *Sol Energy* 1989;42:449-455. [\[CrossRef\]](#)
- [12] Liu GB, Yu KT, Yuan XG, Liu CJ, Guo QC. Simulations of chemical absorption in pilot-scale and industrial-scale packed columns by computational mass transfer. *Chem Engineer Sci* 2006;61:6511-6529. [\[CrossRef\]](#)
- [13] Park MS, Howell JR, Vliet GC, Peterson J. Numerical and experimental results for coupled heat and mass transfer between a desiccant film and air in cross-flow. *Int J Heat Mass Transf* 1994;37:395-402. [\[CrossRef\]](#)
- [14] Ren CQ. Corrections to the simple effectiveness-NTU method for counterflow cooling towers and packed bed liquid desiccant-air contact systems. *Int J Heat Mass Transf* 2008;51:237-245. [\[CrossRef\]](#)
- [15] Luo Y, Shao S, Qin F, Tian C, Yang H. Investigation on feasibility of ionic liquids used in solar liquid desiccant air conditioning system. *Sol Energy* 2012;86:2718-2724. [\[CrossRef\]](#)
- [16] Liu XH, Zhang Y, Qu KY, Jiang Y. Experimental study on mass transfer performances of cross flow dehumidifier using liquid desiccant. *Energy Conver Manage* 2006;47:2682-2692. [\[CrossRef\]](#)
- [17] Tao W, Yimo L, Lin L. A novel 3D simulation model for investigating liquid desiccant dehumidification performance based on CFD technology. *Appl Energy* 2019;240:486-498. [\[CrossRef\]](#)
- [18] Jayanti S, Hewitt GF. Hydrodynamics and heat transfer in wavy annular gas-liquid flow: A computational fluid dynamics study. *Int J Heat Mass Transf* 1997;40:2445-2460. [\[CrossRef\]](#)
- [19] Del Carlo L, Olujić Z, Paglianti A. Comprehensive mass transfer model for distillation columns equipped with structured packings. *Ind Engineer Chem Res* 2006;45:7967-7976. [\[CrossRef\]](#)
- [20] Banerjee R, Bai X, Pugh D, Isaac KM, Klein D, Edson J, et al. CFD simulations of critical components in fuel filling systems. *SAE Tech Pap* 2002-01-0573, 2002. p. 724. [\[CrossRef\]](#)
- [21] Haroun Y, Raynal L, Legendre D. Mass transfer and liquid hold-up determination in structured packing by CFD. *Chem Engineer Sci* 2012;75:342-348. [\[CrossRef\]](#)
- [22] Turgut OE, Çoban MT. Experimental and numerical investigation on the performance of an internally cooled dehumidifier. *Heat Mass Transf* 2016;52:2707-2722. [\[CrossRef\]](#)
- [23] Wen T, Luo Y, He W, Gang W, Sheng L. Development of a novel quasi-3D model to investigate the performance of a falling film dehumidifier with CFD technology. *Int J Heat Mass Transf* 2019;132:431-442. [\[CrossRef\]](#)

- [24] Xu YY, Paschke S, Repke JU, Yuan JQ, Wozny G. Computational approach to characterize the mass transfer between the counter-current gas-liquid flow. *Chem Engineer Technol* 2009;32:1227-1235. [\[CrossRef\]](#)
- [25] Wen T, Lu L. Numerical and experimental study on internally cooled liquid desiccant dehumidification concerning film shrinkage shape and vapor condensation. *Int J Therm Sci* 2019;136:316-327. [\[CrossRef\]](#)
- [26] Luo Y, Shao S, Xu H, Tian C, Yang H. Experimental and theoretical research of a fin-tube type internally-cooled liquid desiccant dehumidifier. *Appl Energy* 2014;133:127-134. [\[CrossRef\]](#)
- [27] Qi R, Lu L. Energy consumption and optimization of internally cooled/heated liquid desiccant air-conditioning system: A case study in Hong Kong. *Energy* 2014;73:801-808. [\[CrossRef\]](#)
- [28] Qi R, Lu L, Yang H, Qin F. Investigation on wetted area and film thickness for falling film liquid desiccant regeneration system. *Appl Energy* 2013;112:93-101. [\[CrossRef\]](#)
- [29] Qi R, Lu L, Jiang Y. Investigation on the liquid contact angle and its influence for liquid desiccant dehumidification system. *Int J Heat Mass Transf* 2015;88:210-217. [\[CrossRef\]](#)
- [30] Bouzenada S, McNevin C, Harrison S, Kaabi AN. An experimental study on the dehumidification performance of a low-flow falling-film liquid desiccant air-conditioner. *Proc Comp Sci* 2015;52:796-803. [\[CrossRef\]](#)
- [31] Dong C, Lu L, Wen T. Experimental study on dehumidification performance enhancement by TiO<sub>2</sub> superhydrophilic coating for liquid desiccant plate dehumidifiers. *Build Environ* 2017;124:219-231. [\[CrossRef\]](#)
- [32] Lu H, Lu L, Luo Y, Qi R. Investigation on the dynamic characteristics of the counter-current flow for liquid desiccant dehumidification. *Energy* 2016;101:229-238. [\[CrossRef\]](#)
- [33] Das A, Das RS, Das K. Performance analysis of aqueous LiCl and CaCl<sub>2</sub> based falling film dehumidifier with surface modification. *Appl Therm Engineer* 2022;200:117704. [\[CrossRef\]](#)
- [34] Das A, Das RS, Das K. Performance enhancement of a liquid desiccant absorber with triangular corrugated structured packing. *J Build Engineer* 2022;45:103677. [\[CrossRef\]](#)
- [35] Lyu Y, Yin Y, Wang J. Effect of air parameters on LiCl-H<sub>2</sub>O film flow behavior in liquid desiccant systems. *Buildings* 2024;14:1474. [\[CrossRef\]](#)
- [36] Das A, Das RS, Das K. Numerical analysis of liquid desiccant dehumidification system with novel trapezoidal baffled surface. *Int J Refrig* 2023;145:457-466. [\[CrossRef\]](#)
- [37] Du B, Zhang G, Xie J, Liu H, Liu J. Experimental analysis of an innovative internally cooled dehumidifier. *J Build Engineer* 2023;80:108057. [\[CrossRef\]](#)
- [38] Du B, Zhang G, Xie J, Liu H, Liu J. Study on the influence characteristics of thermal effect of internally cooled dehumidifier. *Appl Therm Engineer* 2024;236:121850. [\[CrossRef\]](#)
- [39] Gao Y, Lu L. Parametric analysis and multi-objective optimization of a membrane distillation liquid desiccant regenerator with heat/moisture recovery and potable water production. *Energy* 2024;297:131319. [\[CrossRef\]](#)
- [40] Khan R, Neyer D, Kurzina I, Kumar R. Heat and mass transfer characteristics of vertical falling film cylindrical plastic surfaces under partial wetting conditions for liquid desiccant regeneration. *Appl Therm Engineer* 2024;242:122462. [\[CrossRef\]](#)
- [41] Peng D, Li Y, Cheng N. Study on the performance of tube evaporative cooling dehumidifier based on CFD. *Appl Therm Engineer* 2024;241:122419. [\[CrossRef\]](#)
- [42] Rokhman F, et al. Performance enhancement of falling film dehumidifier by variation number and width ratio rectangular cylinder based on CFD simulation. *Int J Heat Mass Transf* 2024;221:125002. [\[CrossRef\]](#)
- [43] Zhao CY, Zhang P, Guan Q, Qi D, Zhang Y, Jiang JM. Numerical study of falling film dehumidification performance on corrugated plates. *Int J Heat Mass Transf* 2024;219:124843. [\[CrossRef\]](#)
- [44] Zhou D, Zhang Y, Zhang Y, Wu Y, Zhang G. Numerical study on the interface characteristics of gas-liquid falling film flow considering the interface forces. *Phys Fluids* 2024;36:0203373. [\[CrossRef\]](#)
- [45] Mondal D, Alam A, Islam MA. Experimental observation of a small capacity vapor absorption cooling system 2014;5:456-467.
- [46] Mondal D, Ikram MO, Rabbi MF, Moral MNA. Experimental investigation and comparison of bend tube parallel & counter flow and cross flow water to air heat exchanger. *Int J Sci Engineer Res* 2014;5:686-695.
- [47] Mondal D, Islam MA. Experimental investigation on an intermittent ammonia absorption refrigeration. *Mech Engineer Res J* 2018;11:59-65.
- [48] Mondal D, Hori Y, Kariya K, Miyara A, Jahangir Alam M. Measurement of viscosity of a binary mixture of R1123 + R32 refrigerant by tandem capillary tube method. *Int J Thermophys* 2020;41:1-20. [\[CrossRef\]](#)
- [49] Mondal D, Kariya K, Tuhin AR, Amakusa N, Miyara A. Viscosity measurement for trans-1,1,1,4,4,4-hexafluoro-2-butene(R1336mzz(E)) in liquid and vapor phases. *Int J Refrig* 2022;133:267-275. [\[CrossRef\]](#)
- [50] Mondal D, Kariya K, Tuhin AR, Miyoshi K, Miyara A. Thermal conductivity measurement and correlation at saturation condition of HFO refrigerant trans-1,1,1,4,4,4-hexafluoro-2-butene (R1336mzz(E)). *Int J Refrig* 2021;129:109-117. [\[CrossRef\]](#)

- [51] Mondal D, Tuhin AR, Kariya K, Miyara A. Measurement of kinematic viscosity and thermal conductivity of 3,3,4,4,5,5-HFCPE in liquid and vapor phases. *Int J Refrig* 2022;140:150-165. [\[CrossRef\]](#)
- [52] Islam L, Mondal D, Islam A, Das P. Effects of heat transfer characteristics of R32 and R1234yf with Al<sub>2</sub>O<sub>3</sub> nanoparticle through U-bend tube evaporator. *J Engineer* 2024;24:9991809. [\[CrossRef\]](#)
- [53] Das P, Mondal D, Islam A, Afroj M. Thermodynamic performance evaluation of a solar powered Organic Rankine cycle (ORC) and dual cascading vapor compression cycle (DCVCC): Power generation and cooling effect. *Energy Convers Manage* 2024;23:100662. [\[CrossRef\]](#)
- [54] Kumar K, Singh A, Chaurasiya PK, Kishore Pathak K, Pandey V. Progressive development in hybrid liquid desiccant-vapour compression cooling system: A review. *Sustain Energy Technol Assess* 2023;55:102960. [\[CrossRef\]](#)
- [55] Zhao CY, Liang LW, Qi D, Ji WT, Tao WQ. The effect of gas streams on the hydrodynamics, heat and mass transfer in falling film evaporation, absorption, cooling and dehumidification: A comprehensive review. *Build Environ* 2022;219:109183. [\[CrossRef\]](#)
- [56] Fahad FG, et al. Advancements in liquid desiccant technologies: A comprehensive review of materials, systems, and applications. *Sustainability* 2023;15:14021. [\[CrossRef\]](#)
- [57] Koronaki IP, Christodoulaki RI, Papaefthimiou VD, Rogdakis ED. Thermodynamic analysis of a counter flow adiabatic dehumidifier with different liquid desiccant materials. *Appl Therm Engineer* 2013;50:361-373. [\[CrossRef\]](#)
- [58] Park JY, Dong HW, Cho HJ, Jeong JW. Energy benefit of a cascade liquid desiccant dehumidification in a desiccant and evaporative cooling-assisted building air-conditioning system. *Appl Therm Engineer* 2019;147:291-301. [\[CrossRef\]](#)
- [59] Mohammad AT, Bin Mat S, Sulaiman MY, Sopian K, Al-Abidi AA. Survey of liquid desiccant dehumidification system based on integrated vapor compression technology for building applications. *Energy Build* 2013;62:1-14. [\[CrossRef\]](#)
- [60] Rafique MM, Gandhidasan P, Bahaidarah HMS. Liquid desiccant materials and dehumidifiers - A review. *Renew Sustain Energy Rev* 2016;56:179-195. [\[CrossRef\]](#)
- [61] Jani DB, Rathod DP, Kureshi F. A review on recent development in liquid desiccant dehumidification assisted cooling systems. *Int J Adv Res Sci Comm Technol* 2022;2:683-690. [\[CrossRef\]](#)
- [62] Misha S, Mat S, Ruslan MH, Sopian K. Review of solid/liquid desiccant in the drying applications and its regeneration methods. *Renew Sustain Energy Rev* 2012;16:4686-4707. [\[CrossRef\]](#)
- [63] Banerjee R, Isaac KM. Evaluation of turbulence closure scheme for stratified two phase flow. ASME 2003 International Mechanical Engineering Congress and Exposition, Washington DC, November 15-21, 2003. pp. 689-705. [\[CrossRef\]](#)
- [64] Lemmon EW, Bell H, Huber IL, McLinden MO. NIST Standard Reference Database 23: Reference Fluid Thermodynamic Properties-REFPROP (DLL Version 10.0a); 2018.